Asociación Argentina
de Mecánica Computacional

Mecánica Computacional Vol XXIX, págs. 2309-2322 (artículo completo)
Eduardo Dvorkin, Marcela Goldschmit, Mario Storti (Eds.)
Buenos Aires, Argentina, 15-18 Noviembre 2010

NUMERICAL SIMULATION OF SEISMOELECTROGRAMS

Patricia M. Gauzellino[a], Juan E. Santos[a,b,c] and Fabio I. Zyserman[a,b]

[a]*Depto. Geofísica Aplicada, Fac. de Cs. Astronómicas y Geofísicas, UNLP, Paseo del Bosque s/n, 1900 La Plata, Argentina, gauze@fcaglp.unlp.edu.ar*

[b]*CONICET, Argentina*

[c]*Department of Mathematics, Purdue University, 150 N. University Street, West Lafayette, Indiana, 47907-2067, USA*

Keywords: Seismoelectric modeling, Poroelasticity, Electromagnetics, Finite element methods.

Abstract. The conversion of energy between seismic and electromagnetic wave fields involves relative movement of ions at the rock-fluid contact surfaces in the pore space, described by Biot's equations of motion in poroviscoelastic media coupled with Maxwell's equations. The numerical simulation of seismoelectrograms allows to analyze full-waveform coupled seismoelectromagnetic wave propagation in fluid-saturated porous media. It is possible to observe two different responses: the coseismic response with the same waveform as a seismic wave and the interface response that occurs when a seismic wave encounters a contrast in electrical or mechanical material properties. The proposed algorithm calculates the electromagnetic field from seismic displacements, particularly fluid displacements, using the finite element method employing a parallelizable non-overlapping domain decomposition technique, which is required due to the high computational cost of the problem. The seismoelectric method allows the possibility of detecting very thin impermeable layers, permeable fractures and interfaces between different formations due to changes in permeability or saturant fluids. The 2D implementation of the procedure illustrates identification of subsurface heterogeneities when applied to different targets and source-receiver configurations.

1 INTRODUCTION

Seismic waves propagating through near-surface layers of the Earth may induce electromagnetic disturbances that can be measured at the surface (seismoelectric effect) (Pride and Haartsen, 1996; Mikhailov et al., 1997, 2000). Also, recent tests suggest that the reciprocal process, *i.e.* surface measurable acoustic disturbances induced by electromagnetic fields (electroseismic effect), is also possible (Thompson, 2005; Hornbostel and Thompson, 2007).
In order to explain these phenomena, Thompson and Gist (Thompson and Gist, 1993) and Pride (Pride, 1994) suggested that they are generated by an electrokinetic coupling mechanism which can be shortly explained as follows (Block and Harris, 2006; Haines and Pride, 2006). Within a fluid saturated porous medium there exists a nanometer-scale separation of electric charge in which a bound charge existing on the surface of the solid matrix (normally of negative sign) is balanced by adsorbed positive ions of the surrounding fluid, setting an immobile layer. Further from the surface there exists a distribution of mobile counter ions, forming the so called diffuse layer. The effective thickness of this double layer is of about 10 nm. When an electric field is applied to this system, the ions in the diffuse layer move, dragging the pore fluid along with it because of the viscous traction. This is known as electro-osmosis and is responsible for the electroseismic phenomena. On the other hand, the reciprocal situation arises when an applied pressure gradient creates fluid flow and hence, an ionic convection current, which in turn produces an electric field. This is known as electrofiltration and is responsible for the so-called seismoelectric phenomena.
Using a volume averaging approach, Pride (Pride, 1994) derived a set of equations describing both electroseismic and seismoelectric effects in electrolyte-saturated porous media. In these equations the coupling mechanism acts through the (generally frequency dependent) electrokinetic coupling coefficient $L(\omega)$. When this coefficient is set to zero, Pride's set of equations turns to the uncoupled Maxwell's and Biot's equations, describing the latter mechanical wave propagation in a fluid saturated porous medium (**?**Biot, 1956b).
There exist already some works implementing different numerical methods to solve the set of equations modeling both mentioned processes. Haartsen and Pride (Haartsen and Pride, 1997), Han and Wang (Han and Wang, 2001), Pain et. al (Pain et al., 2005), Haines and Pride (Haines and Pride, 2006) and White (White, 2005) and White and Zhou (White and Zhou, 2006) have proposed several different approaches to numerically study these phenomena.
The objective of this paper is to define a finite element procedure, stated in the space-frequency domain, for the approximate solution of Maxwell's and Biot's equations of motion in an isotropic bounded domain, with absorbing boundary conditions at the artificial boundaries. The case analyzed is that of compressional and vertically polarized seismic waves coupled with the transverse magnetic polarization (PSVTM-mode). The vector electric field and the scalar magnetic field are computed using the rotated Raviart-Thomas-Nedelec spaces of zero order (Raviart and Thomas, 977; Nedelec, 1980). Also, the nonconforming space defined in (Douglas Jr. et al., 1999) is used to approximate each component of the displacement vector in the solid phase, while the displacement in the fluid phase is approximated using the vector part of the Raviart-Thomas-Nedelec mixed finite element space of zero order.

2 THE DIFFERENTIAL MODEL

Consider a 2D-rectangular domain $\Omega = \Omega_a \cup \Omega_p$ where Ω_a and Ω_p are associated with the air and subsurface poroviscoelastic (disjoint) parts of Ω, respectively. We will assume that (in cartesian coordinates (x_1, x_2, x_3)) all physical quantities describing our domains Ω_a and Ω_p are

independent of the x_2-direction (i.e., x_2 is the symmetry axis) and consider a seismic line source in the x_2-direction. Including the air region allows us to include in implicit fashion the boundary conditions for the electromagnetic fields at the air-poroelastic interface.

Let the Fourier transform in the time variable of a given function $f(t)$ be defined as usual by

$$\widehat{f}(\omega) = \int_{-\infty}^{\infty} e^{-i\omega t} f(t) dt.$$

Let us denote by $E(\omega), H(\omega)$ to the electric and magnetic fields in Ω, respectively, and by $u^s(\omega), u^f(\omega)$ to the solid and relative fluid displacement vectors in Ω_p (the $\widehat{\cdot}$ is omitted in all variables for notational convenience).

Under the above symmetry asumption, this source term induces electric and magnetic fields of the form $(E_1(x_1, x_3, t), 0, E_3(x_1, x_3, t))$, $(0, H_2(x_1, x_3, t), 0)$, respectively, and solid and relative fluid displacements of the form $u^s = (u_1^s(x_1, x_3, t), 0, u_3^s(x_1, x_3, t))$ and $u^f = (u_1^f(x_1, x_3, t), 0, u_3^f(x_1, x_3, t))$, respectively. Consequently only compressional and vertically polarized shear seismic waves (PSV-waves) are generated. This is a 2D model known as a PSVTM-mode.

Let us identify the 3D vectors $(E_1(x_1, x_3, t), 0, E_3(x_1, x_3, t))$ and $(0, H_2(x_1, x_3, t)), 0)$ with the 2D vector $(E(x_1, x_3, t) = (E_1(x_1, x_3, t), E_3(x_1, x_3, t))$ and the scalar $H_2(x_1, x_3, t)$, respectively. Then recall that

$$\text{curl } H_2 = \left(-\frac{\partial H_2}{\partial x_3}, \frac{\partial H_2}{\partial x_1} \right), \quad \text{curl } E = \frac{\partial E_1}{\partial x_3} - \frac{\partial E_3}{\partial x_1}.$$

Also, let us identify our 3D-rectangular domain Ω with the 2D-rectangular domain $\Omega \cap \{y = 0\}$, so that Ω is the union of the disjoint rectangular subdomains Ω_a and Ω_p. Let Γ denote the boundary of Ω and let $\Gamma_{a,p} = \overline{\Omega}_a \cap \overline{\Omega}_p$ denote the free surface. Also let $\Gamma_a = \partial\Omega_a \setminus \Gamma_{a,p}$, $\Gamma_p = \partial\Omega_p \setminus \Gamma_{a,p}$ denote the artificial boundaries of Ω_a and Ω_p, respectively.

Following Pride (1994); Haines and Pride (2006), for 2D seismoelectric modeling the electric and magnetic fields E and H and the displacement vectors u^s and u^f satisfy the coupled electromagnetic-poroelastic equations, stated in the space-frequency domain as follows:

$$i\omega\varepsilon E + \sigma E - \text{curl } H_2 + L_0 \frac{\eta}{\kappa_0} i\omega u^f = 0, \quad \Omega, \tag{1}$$

$$\text{curl } E + i\omega H_2 = 0, \quad \Omega, \tag{2}$$

$$-\omega^2 \rho_b u^s - \omega^2 \rho_f u^f - \nabla \cdot \tau(u) = F^{(s)}, \quad \Omega_p, \tag{3}$$

$$-\omega^2 \rho_f u^s - \omega^2 m u^f + i\omega \frac{\eta}{\kappa_0} u^f + \nabla p_f = F^{(f)}, \quad \Omega_p, \tag{4}$$

$$\tau_{lm}(u) = 2G\, \varepsilon_{lm}(u^s) + \delta_{lm} \left(\lambda_c \nabla \cdot u^s + \alpha K_{av} \nabla \cdot u^f \right), \quad \Omega_p, \tag{5}$$

$$p_f(u) = -\alpha K_{av} \nabla \cdot u^s - K_{av} \nabla \cdot u^f, \quad \Omega_p. \tag{6}$$

In the equations above $u = (u^s, u^f)$ and $\tau_{lm}(u)$ is the stress tensor of the bulk material and $p_f(u)$ the fluid pressure, while $\varepsilon_{lm}(u^s)$ denotes the strain tensor of the solid frame.

In order to introduce viscoelasticity, the coefficients in the constitutive equations (5) and (6) are considered to be frequency dependent. They can be determined as follows. First we consider the (relaxed) elastic limits of these coefficients, denoted by the superindex *. In this case, the coefficient G^* is equal to the elastic shear modulus of the dry matrix. Also,

$$\lambda_c^* = K_c^* - G^*, \tag{7}$$

with K_c^* being the bulk modulus of the saturated material. The coefficients in (5)-(6) can be obtained from the relations (Gassmann, 1951; Santos et al., 1992)

$$\alpha = 1 - \frac{K_m}{K_s}, \qquad K_{av}^* = \left[\frac{\alpha - \phi}{K_s} + \frac{\phi}{K_f}\right]^{-1} \tag{8}$$
$$K_c^* = K_m + \alpha^2 K_{av}^*,$$

where K_s, K_m and K_f denote the bulk modulus of the solid grains composing the solid matrix, the dry matrix and the saturant fluid, respectively. Next, using the correspondence principle stated by M. Biot (Biot, 1956a, 1962), we replace the (real) relaxed elastic coefficients G^*, K_c^* and K_{av}^* by complex frequency dependent viscoelastic modulus using the linear viscoelastic model presented in (Liu et al., 1976) as follows:

$$K_c(\omega) = \frac{K_c^*}{R_{K_c}(\omega) - iT_{K_c}(\omega)}, \qquad G(\omega) = \frac{G^*}{R_G(\omega) - iT_G(\omega)}, \tag{9}$$
$$K_{av}(\omega) = \frac{K_{av}^*}{R_{K_{av}}(\omega) - iT_{K_{av}}(\omega)}.$$

The frequency dependent coefficient $\lambda_c = \lambda_c(\omega)$ in (5) is defined in terms of $K_c(\omega)$ and $G(\omega)$ as

$$\lambda_c = K_c(\omega) - G(\omega). \tag{10}$$

Also, the frequency dependent functions R_s and T_s, $s = K_c, G, K_{av}$, associated with a continuous spectrum of relaxation times, characterize the viscoelastic behavior and are given by Liu et al. (1976)

$$R_s(\omega) = 1 - \frac{1}{\pi Q_{m,s}} \ln \frac{1 + \omega^2 T_1^2}{1 + \omega^2 T_2^2}, \qquad T_s(\omega) = \frac{2}{\pi Q_{m,s}} \tan^{-1} \frac{\omega(T_1 - T_2)}{1 + \omega^2 T_1 T_2}.$$

The model parameters $Q_{m,s}, s = K_c, G, K_{av}$, T_1 and T_2 are taken such that the quality factor

$$\widehat{Q}_s(\omega) = \frac{T_s(\omega)}{R_s(\omega)}$$

is approximately equal to the constant $Q_{m,s}$ in the range of frequencies where the equations are solved, which makes this model convenient for geophysical applications. Values of $Q_{m,s}$ range from $Q_{m,s} = 10$ for highly dissipative materials to about $Q_{m,s} = 1000$ for almost elastic ones.

Also, ε is the electric permitivity, μ the magnetic permeability and σ the conductivity, while $F^{(s)}$, $F^{(f)}$ are the external seismic sources. Furthermore,

$$\rho_b = \phi\rho_f + (1 - \phi)\rho_s, \tag{11}$$

where ρ_s and ρ_f denote the mass densities of the solid grains composing the solid matrix and the saturant fluid. On the other hand, η is the fluid viscosity, κ_0 the permeability and m is the mass coupling coefficient between the solid and fluid phases in Ω_p. The mass coupling coefficient m can be written in the form

$$m = \frac{\alpha_\infty \rho_f}{\phi}, \tag{12}$$

with α_∞ being the formation tortuosity.

The positive coupling coefficient L_0 is defined by Haartsen and Pride (1997) as

$$L_0 = -\frac{\phi}{\alpha_\infty}\frac{\epsilon_0 k_f \zeta}{\eta}\left(1 - 2\alpha_\infty \frac{\widetilde{d}}{\Lambda}\right), \tag{13}$$

with $\zeta = 0.008 + 0.026\log_{10}(C_e)$ denoting the zeta potential and C_e being the electrolyte molarity. In (13) ϵ_0 and k_f are the vacuum and fluid permitivities and

$$\widetilde{d} = \frac{\epsilon_0 k_f k_B T}{e^2 z^2 N_{ic}} \tag{14}$$

is the Debye length in meters. in (14) e is the electronic charge, k_B is the Boltzman constant, T is the absolute temperature (so that $k_B T$ is the thermal energy) z is the ionic valence and N_{ic} the ionic concentration in ions per meters cubed.

To solve equations (1)-(6) in our 2D domain Ω we need a collection of boundary conditions. Let Γ denote the boundary of Ω and let $\Gamma_{a,p} = \overline{\Omega}_a \cap \overline{\Omega}_p$ denote the free surface. Also let $\Gamma_a = \partial\Omega_a \setminus \Gamma_{a,p}$, $\Gamma_p = \partial\Omega_p \setminus \Gamma_{a,p}$ denote the artificial boundaries of Ω_a and Ω_p, respectively. Also, if Γ_s is either an inner interface in Ω or a part of the boundaries Γ, Γ_p or $\Gamma_{a,p}$, set

$$\mathcal{G}_{\Gamma_s}(u) = \Big(\tau(u)\nu\cdot\nu, \tau(u)\nu\cdot\chi, p_f(u)\Big)^t, \tag{15a}$$

$$S_{\Gamma_s}(u) = \big(u^s\cdot\nu, u^s\cdot\chi, u^f\cdot\nu\big)^t, \tag{15b}$$

where ^{t} denotes the transpose, ν is the unit outer normal on Γ_s and χ is a unit tangent on Γ_s oriented counterclockwise.

Then, for $\omega > 0$ consider the solution of (1)-(6) with the absorbing boundary conditions (Sheen, 1997; Santos et al., 1998)

$$-\varepsilon^{1/2} E\cdot\chi + H_2 = 0, \quad \text{on} \quad \Gamma, \tag{16}$$

$$-\mathcal{G}_{\Gamma_p}(u) = \mathcal{D} S_{\Gamma_p}\Big(\frac{\partial u}{\partial t}\Big), \quad \text{on} \quad \Gamma_p, \tag{17}$$

and the free surface condition

$$-\mathcal{G}_{\Gamma_p}(u) = 0, \quad \text{on} \quad \Gamma_{a,p}. \tag{18}$$

The matrix $\mathcal{D}$ in (17) is defined as: $\mathcal{D} = \mathcal{R}^{\frac{1}{2}}\mathcal{S}^{\frac{1}{2}}\mathcal{R}^{\frac{1}{2}}$, where $\mathcal{S} = \mathcal{R}^{-\frac{1}{2}}\mathcal{M}^{\frac{1}{2}}\mathcal{R}^{-\frac{1}{2}}$ and

$$\mathcal{R} = \begin{pmatrix} \rho_b & 0 & \rho_f \\ 0 & b & 0 \\ \rho_f & 0 & \zeta \end{pmatrix}, \quad \mathcal{M} = \begin{pmatrix} \lambda_c^* + 2G^* & 0 & \alpha\, K_{av}^* \\ 0 & G^* & 0 \\ \alpha\, K_{av}^* & 0 & K_{av}^* \end{pmatrix}, \tag{19}$$

where

$$b = \rho_b - \frac{(\rho_f)^2}{m}.$$

*R*emark: Note that since $\alpha_\infty \geq 1$, the matrix $\mathcal{R}$ is positive definite. Also, we will requiere that the following conditions be satisfied by the coefficients defining the matrix $\mathcal{M}$:

$$G^* > 0, \tag{20a}$$

$$\lambda_c^* + 2G^* - \alpha^2 K_{av}^* > 0, \tag{20b}$$

$$K_{av}^* > 0. \tag{20c}$$

Conditions (20) are necessary and sufficient conditions for the matrix $\mathcal{M}$ to be positive definite. In particular, the second condition of (20) imposes that the inverse of the jacketed compressibility coefficient be strictly positive, see (Biot, 1962). As a consequence of the positive definitess of the matrices $\mathcal{R}$ and $\mathcal{M}$, the matrix $\mathcal{D}$ is also positive definite.

3 A WEAK FORMULATION

For $X \subset \mathbb{R}^d, d = 1, 2, 3$ with boundary ∂X, let $(\cdot,\cdot)_X$ denote the complex $L^2(X)$ inner product for scalar, vector, or matrix valued functions. Also, for $s \in \mathbb{R}$, $\|\cdot\|_{s,X}$ will denote the usual norm for the Sobolev space $H^s(X)$. In addition, if $X = \Omega$ or $X = \Gamma$, the subscript X may be omitted such that $(\cdot,\cdot) = (\cdot,\cdot)_\Omega$ or $\langle\cdot,\cdot\rangle = \langle\cdot,\cdot\rangle_\Gamma$. Set

$$
\begin{aligned}
H(\text{curl},\Omega) &= \{\psi \in (L^2(\Omega))^2 : \text{curl}\psi \in L^2(\Omega)\},\\
H(\text{div},\Omega_p) &= \{\psi \in (L^2(\Omega_p))^2 : \nabla\cdot\psi \in L^2(\Omega_p)\},\\
H^1(\text{div},\Omega) &= \{\psi \in (H^1(\Omega))^2 : \nabla\cdot\psi \in H^1(\Omega)\}
\end{aligned}
$$

provided with the natural norms

$$
\begin{aligned}
\|\psi\|_{H(\text{curl},\Omega)} &= (\|\psi\|_0^2 + \|\text{curl}\psi\|_0^2)^{\frac{1}{2}},\\
\|\psi\|_{H(\text{div},\Omega_p)} &= (\|\psi\|_{0,\Omega_p}^2 + \|\nabla\cdot\psi\|_{0,\Omega_p}^2)^{\frac{1}{2}},\\
\|\psi\|_{H^1(\text{div},\Omega} &= (\|\psi\|_1^2 + \|\nabla\cdot\psi\|_1^2)^{\frac{1}{2}}.
\end{aligned}
$$

Recall the integration by parts formulas (Girault and P., 1986; Sheen, 1992)

$$
(\psi, \text{curl}\varphi) - (\text{curl}\,\psi,\varphi) = \langle\psi\cdot\chi,\varphi\rangle\,, \quad \forall\psi \in H(\text{curl},\Omega), \quad \varphi \in H^1(\Omega), \tag{21}
$$

$$
(\nabla\cdot\psi,\varphi) + (\psi,\nabla\varphi) = \langle\psi\cdot\nu,\varphi\rangle\,, \quad \forall\psi \in H(\text{div},\Omega), \quad \varphi \in H^1(\Omega). \tag{22}
$$

To obtain a variational formulation, test (2) against $\varphi \in L^2(\Omega)$ and test (1) against $\psi \in H(\text{curl},\Omega)$ and use the integration by parts formula (21) and the boundary condition (16) to obtain the equations

$$
\begin{aligned}
(i\omega\varepsilon Et,\psi) + (\sigma E,\psi) - (H_2,\text{curl}\,\psi) + \left(i\omega L_0\frac{\eta}{\kappa_0}u^f,\psi\right)_{\Omega_p} \\
+ \left\langle\left(\frac{\varepsilon}{\mu}\right)^{1/2}E\cdot\chi,\psi\cdot\chi\right\rangle = 0, \quad \psi \in H(\text{curl},\Omega),
\end{aligned} \tag{23}
$$

$$
(\text{curl}\,E,\varphi) + (i\omega\mu H_2,\varphi) = 0, \quad \varphi \in L^2(\Omega). \tag{24}
$$

Next, test (3) against $v^s \in [H^1(\Omega_p)]^2$ and (4) against $v^f \in H(\text{div},\Omega_p)$ and use the integration by parts formula (22) and the boundary condition (17). Setting

$$
\mathcal{P} = \begin{pmatrix} \rho_b I_2 & \rho_f I_2 \\ \rho_f I_2 & m I_2 \end{pmatrix} \tag{25}
$$

where I_2 is the identity matrix in R^2 we get the equation

$$
\begin{aligned}
-(\omega^2\mathcal{P}ut,v)_{\Omega_p} + (i\omega\frac{\eta}{\kappa_0}u^f t,v^f)_{\Omega_p} + \mathcal{A}(u,v) + \left\langle i\omega\mathcal{D}S_{\Gamma_p}u, S_{\Gamma_p}(v)\right\rangle_{\Gamma_p} \\
= (F,v)_{\Omega_p}, \quad v = (v^s,v^f) \in [H^1(\Omega_p)]^2 \times H(\text{div},\Omega_p).
\end{aligned} \tag{26}
$$

In (26) $F = (F^s, F^f)$ and $A(u, v)$ is the bilinear form defined as

$$\mathcal{A}(u,v) = \sum_{l,m} (\tau_{lm}(u), \varepsilon_{lm}(v^s))_{\Omega_p} - \left(p_f(u), \nabla \cdot v^f\right)_{\Omega_p} = (\mathbf{M}\,\widetilde{\epsilon}(u), \widetilde{\epsilon}(v))_{\Omega_p}\,,$$
$$u, v \in [H^1(\Omega_p)]^2 \times H(\mathrm{div}, \Omega_p), \tag{27}$$

where the complex matrix $\mathbf{M} = \mathbf{M}_r(\omega) + i\mathbf{M}_i(\omega)$ in (27) is given by

$$\mathbf{M} = \begin{pmatrix} \lambda_c + 2G & \lambda_c & \alpha\, K_{av} & 0 \\ \lambda_c & \lambda_c + 2G & \alpha\, K_{av} & 0 \\ \alpha\, K_{av} & \alpha\, K_{av} & K_{av} & 0 \\ 0 & 0 & 0 & 4G \end{pmatrix}, \tag{28}$$

and $\widetilde{\varepsilon}(u) = \left(\varepsilon_{11}(u^{(s)}), \varepsilon_{22}(u^{(s)}), \nabla \cdot u^{(f)}, \varepsilon_{12}(u^{(s)})\right)^t$.

Note that the matrix $\mathcal{P}$ is positive definite. Furthermore, we assume that the real part $\mathbf{M}_r$ is positive definite since in the elastic limit it is associated with the strain energy density. On the other hand, the imaginary part $\mathbf{M}_i$ is assumed to be positive definite because of the restriction imposed on our system by the First and Second Laws of Thermodynamics (Ravazzoli and Santos, 2005).

Let

$$\mathcal{Y} = (\mathrm{curl}, \Omega) \times L^2(\Omega) \times [H^1(\Omega_p)]^2 \times H(\mathrm{div}, \Omega_p).$$

Our weak formulation is stated as follows: for $\omega > 0$, find $(E, H_2, u^s, u^f) \in \mathcal{Y}$ satisfying (23), (24) and (26).

The uniqueness of the solution of (23), (24) and (26) can be demonstrated with an argument similar to that given in (Santos, 2010).

4 A FINITE ELEMENT METHOD FOR THE PSVTM-MODE. RECTANGULAR ELEMENTS

Let $\mathcal{T}^h(\Omega)$ be a nonoverlapping quasiregular partition of $\Omega = \Omega_p \cup \Omega_a$ into rectangles Ω_j of diameter bounded by h such that $\overline{\Omega} = \cup_{j=1}^{J} \overline{\Omega}_j$. Denote by ξ_j and ξ_{jk} the midpoints of $\Gamma_j = \partial\Omega_j \cap \Gamma$ and $\Gamma_{jk} = \Gamma_{kj} = \partial\Omega_j \cap \partial\Omega_k$, respectively.

To approximate the electromagnetic fields E, H_2 we will employ the mixed finite element space $\mathcal{V}^h \times \mathcal{W}^h$, defined as follows (Nedelec, 1980; Monk and Parrot, 1994):

$$\mathcal{V}^h = \{\psi \in H(\mathrm{curl}, \Omega) : \psi|\Omega_j \in \mathcal{V}_j^h \equiv P_{0,1}(\Omega_j) \times P_{1,0}(\Omega_j)\},$$
$$\mathcal{W}^h = \{\varphi \in L^2(\Omega) : \varphi|\Omega_j \in \mathcal{W}_j^h \equiv P_0(\Omega_j)\}.$$

Here, $P_{s,t}(\Omega_j)$ denote the polynomials of degree not greater than s in x and not greater than t in z on Ω_j, while P_0 denote the constants on Ω_j. The functions in $\mathcal{V}^h$ have continuous tangential components across the internal boundaries Γ_{jk}. Also, curl$\mathcal{V}^h \subset \mathcal{W}^{(h)}$.

Following Monk and Parrot (1994), the degrees of freedom for $\mathcal{V}^h$ are defined in the following way. Let Ω_j be a general element of the partition $\mathcal{T}^h(\Omega)$ and let $\psi \in [H^1(\Omega_j)]^2$. Then define the following moments on Γ_{jk}:

$$M_{\Gamma_{jk}}(\psi) = \left\{ \langle \psi \cdot \tau, f \rangle_{\Gamma_{jk}}\,; \quad f \in P_0(\Gamma_{jk}) \right\}. \tag{29}$$

Note that (29) are curl–conforming and unisolvent for elements in $\mathcal{V}^h$.

To approximate each component of the solid displacement vector we employ the nonconforming finite element space $\mathcal{NC}^h$ as in Douglas Jr. et al. (1999), while to approximate the fluid displacement vector we choose $\mathcal{M}^h$, the vector part of the Raviart-Thomas-Nedelec space (Raviart and Thomas, 977; Nedelec, 1980) of zero order. More precisely, set

$$\widehat{R} = [-1,1]^2, \qquad \widehat{\mathcal{NC}}(\widehat{R}) = \text{Span}\{1, \widehat{x}_1, \widehat{x}_3, \widetilde{\alpha}(\widehat{x}_1) - \widetilde{\alpha}(\widehat{x}_3)\}, \quad \widetilde{\alpha}(\widehat{x}_1) = \widehat{x}_1^2 - \frac{5}{3}\widehat{x}_1^4.$$

with the degrees of freedom being the values at the midpoint of each edge of $\widehat{R}$. Next, for each $\Omega_j \subset \Omega_p$, let $F_{\Omega_j} : \widehat{R} \to \Omega_j$ be an invertible affine mapping such that $F_{\Omega_j}(\widehat{R}) = \Omega_j$, and define

$$\mathcal{NC}_j^h \;=\; \{v : v = \widehat{v} \circ F_{\Omega_j}^{-1}, \, \widehat{v} \in \widehat{\mathcal{NC}}(\widehat{R})\}.$$

Thus,

$$\mathcal{NC}^h = \{v \, : v_j = v|_{\Omega_j} \in \mathcal{NC}_j^h, \; v_j(\xi_{jk}) = v_k(\xi_{jk}) \; \forall (j,k)\},$$
$$\mathcal{M}^h = \{w \in H(\text{div}, \Omega_p) : w|\Omega_j \in \mathcal{M}_j^h \equiv P_{1,0}(\Omega_j) \times P_{0,1}(\Omega_j)\}.$$

To state the approximating properties of the finite element spaces defined above we introduce the following four projection operators.

First, let

$$[H_h^1(\Omega)]^2 = \{\psi : \psi|\Omega_j \in [H^1(\Omega_j)]^2\},$$

with $[H_h^1(\Omega_p)]^2$ defined in similar fashion and if $\Gamma_{jk,p}$ denotes any inner interface Γ_{jk} in Ω_p let

$$\widetilde{\Lambda}^h = \left\{\widetilde{\lambda}^h : \widetilde{\lambda}_{jk}^h = \text{tr}_{\,\Gamma_{jk,p}}(\widetilde{\lambda}^h|_{\Omega_j}) \in [P_0(\Gamma_{jk,p})]^2 \equiv \widetilde{\Lambda}_{jk}^h, \quad \widetilde{\lambda}_{jk}^h + \widetilde{\lambda}_{kj}^h = 0\right\},$$

where $P_0(\Gamma_{jk,p})$ denotes the constant functions defined on $\Gamma_{jk,p}$.

*R*emark: Note that there are two copies of $[P_0(\Gamma_{jk,p})]^2$ assigned to each $\Gamma_{jk,p}$, one from Ω_j to Ω_k and another from Ω_k to Ω_j.

Then we define the projections

$$\Pi_h : H(\text{curl}, \Omega) \cap [H_h^1(\Omega)]^2 \to \mathcal{V}^h : \langle(\psi - \Pi_h\psi)\cdot\chi, 1\rangle_B = 0, \; B = \Gamma_{jk} \text{ or } \Gamma_j, \tag{30}$$
$$P_h : L^2(\Omega) \to \mathcal{W}^h : \qquad (P_h w - w, \varphi) = 0, \; \varphi \in \mathcal{W}^h, \tag{31}$$
$$R_h : [H^2(\Omega_p)]^2 \to [\mathcal{NC}^h]^2 : \qquad (v_i^s - R_h v_i^s)(\xi) = 0, \; \xi = \xi_{jk} \text{ or } \xi_j, \tag{32}$$
$$\text{for} \quad v^s = (v_1^s, v_2^s),$$
$$Q_h : [H^1(\Omega_p)]^2 \to \mathcal{M}^h : \qquad \left\langle(v^f - Q_h v^f)\cdot\nu, 1\right\rangle_B = 0; \; B = \Gamma_{jk,p} \text{ or } \Gamma_j, \tag{33}$$
$$S_h : [H^2(\Omega_p)]^2 \times H^1(\text{div}; \Omega_p) \to \widetilde{\Lambda}^h : \qquad \langle\tau(v)\nu - S_h(v), 1\rangle_B = 0, \tag{34}$$
$$v = (v^s, v^f), B = \Gamma_{jk,p} \text{ or } \Gamma_j.$$

Let us define the broken norms

$$\|v\|_{s,h,\Omega_p}^2 = \sum_{\Omega_j \subset \Omega_p} \|v\|_{s,\Omega_j}^2.$$

The approximation properties of these operators can be stated as follows (Nedelec, 1980; Santos and Sheen, 2007):

$$\|\psi - \Pi_h\psi\|_0 \leq Ch\|\psi\|_1,\ \psi \in [H^1(\Omega)]^2, \tag{35}$$

$$\|\text{curl}(\psi - \Pi_h\psi)\|_0 \leq Ch\|\text{curl}\ \psi\|_1,\ \psi \in [H^1(\Omega)]^2,\ \text{curl}\psi \in H^1(\Omega), \tag{36}$$

$$\|P_h\varphi - \varphi\|_0 \leq Ch\|\varphi\|_1, \qquad \forall\varphi \in H^1(\Omega), \tag{37}$$

$$\begin{aligned}&\Big[\|v^s - R_h v^s\|_{\Omega_p} + h\|v^s - R_h v^s\|^2_{1,h,\Omega_p} + h^2\|v^s - R_h v^s\|^2_{2,h,\Omega_p}\\ &\quad + h^{\frac{1}{2}}\Big(\sum_{\Omega_j\subset\Omega_p}\|v^s - R_h v^s\|^2_{0,\partial\Omega_j}\Big)^{\frac{1}{2}} + h^{\frac{3}{2}}\Big(\sum_{\Omega_j\subset\Omega_p}\|\tau(v_j)\nu_j - S_h v_j\|^2_{0,\partial\Omega_j}\Big)^{1/2}\\ &\leq Ch^2\left(\|v^s\|_{2,\Omega_p} + \|\nabla\cdot v^f\|_{1,\Omega_p}\right),\ v = \left(v^s, v^f\right) \in [H^2(\Omega_p)]^2 \times H^1(\text{div},\Omega_p),\end{aligned} \tag{38}$$

$$\|Q_h v^f - v^f\|_{0,\Omega_p} \leq Ch\|\mathbf{v}^f\|_{1,\Omega_p},\ v^f \in [H^1(\Omega_p)]^2, \tag{39}$$

$$\|\nabla\cdot(v^f - Q_h v^f)\|_{0,\Omega_p} \leq Ch\|\nabla\cdot v^f\|_{1,\Omega_p},\ v^f \in H^1(\text{div},\Omega_p). \tag{40}$$

Note that since curl $\psi \in \mathcal{W}^h\ \forall\psi \in \mathcal{V}^h$, it follows from (31) that

$$(P_h f - f, \text{curl}\ \psi) = 0, \quad \forall\psi \in \mathcal{V}^h. \tag{41}$$

Also note the orthogonality property for functions on $\mathcal{NC}^h$:

$$\left\langle v^s_j - v^s_k, 1\right\rangle_{\Gamma_{jk}} = 0 \text{ for all interior interfaces } \Gamma_{jk}, \quad v^s \in \mathcal{NC}^h. \tag{42}$$

Set

$$\begin{aligned}\mathcal{A}_h(u,v) &= \sum_{\Omega_j\subset\Omega_p}\left[\sum_{l,m}\left(\tau_{lm}(u), \varepsilon_{lm}(v^{(s)})\right)_{\Omega_j} - \left(p_f(u), \nabla\cdot v^f\right)_{\Omega_j}\right]\\ &= \sum_{\Omega_j\subset\Omega_p}\left(\mathbf{M}\,\widetilde{\epsilon}(u), \widetilde{\epsilon}(v)\right)_{\Omega_j},\end{aligned} \tag{43}$$

and

$$\begin{aligned}\Theta_h\left((E, H_2, u^s, u^f), (\psi, \varphi, v^s, v^f)\right) &= (\varepsilon\frac{\partial E}{\partial t}, \psi) + (\sigma E, \psi) - (H_2, \text{curl}\psi)\\ &+ \left(L_0\frac{\eta}{\kappa_0}\frac{\partial u^f}{\partial t}, \psi\right)_{\Omega_p} + (\text{curl}E, \varphi) + \left\langle\left(\frac{\varepsilon}{\mu}\right)^{1/2} E\cdot\chi, \psi\cdot\chi\right\rangle\\ &+ (\mu\frac{\partial H_2}{\partial t}, \varphi) + \left(\mathcal{P}\frac{\partial^2 u}{\partial t^2}, v\right)_{\Omega_p} + \left(\frac{\eta}{\kappa_0}\frac{\partial u^f}{\partial t}, v^f\right)_{\Omega_p} + \mathcal{A}_h(u,v) + \left\langle\mathcal{D}S_\Gamma(\frac{\partial u}{\partial t}), S_\Gamma(v)\right\rangle_{\Gamma_p}.\end{aligned} \tag{44}$$

Let

$$\mathcal{Y}^h = \mathcal{V}^h \times \mathcal{W}^h \times (\mathcal{NC}^h)^2 \times \mathcal{M}^h.$$

The Galerkin procedure is defined as follows: find $\left(E^h, H_2^h, u^{s,h}, u^{f,h}\right) \in \mathcal{Y}^h$ such that

$$\begin{aligned}\Theta_h\left((E^h, H_2^h, u^{s,h}, u^{f,h}), (\psi, \varphi, v^s, v^f)\right) &= (F^s, v^s)_{\Omega_p} + (F^f, v^f)_{\Omega_p},\\ (\psi, \varphi, v^s, v^f) &\in \mathcal{Y}^h.\end{aligned} \tag{45}$$

Uniqueness for (45) follows with the same argument than for (23), (24) and (26); existence will be assumed. The following *apriori* error estimate can be demosntrated using the ideas presented in (Santos, 2010).

Theorem 1 *Let* $(E, H_2, u^s, u^f) \in \mathcal{Y}$ *be the solution of* (23), (24) *and* (26) *and let* $(E^h, H_2^h, u^{s,h}, u^{f,h}) \in \mathcal{Y}^h$ *be the solution of* (45), *respectively. Assume that* $E \in [H^1(\Omega)]^2$, *curl* E, $\mathbf{H}_2 \in H^1(\Omega)$ $u^s \in [H^2(\Omega_p)]^2$, $u^f \in H^1(div, \Omega_p)$. *Also assume that the matrix* $\mathbf{M}_i$ *is positive definite. Then the following a priori error estimate holds: for* $\omega > 0$ *and* $h > 0$ *sufficiently small,*

$$\begin{aligned}
&\|E - E^h\|_0 + \|curl(E - E^h)\|_0 + \|H_2 - H_2^h\|_0 + \|u^s - u^{s,h}\|_{1,h,\Omega_p} + \|u^f - u^{f,h}\|_{0,\Omega_p} \\
&+\|\nabla \cdot (u^f - u^{f,h})\|_{0,\Omega_p} + \|(E - E^h) \cdot \chi\|_{0,\Gamma} + \|u^s - u^{s,h}\|_{0,\Gamma_p} + \|(u^f - u^{f,h}) \cdot \nu\|_{0,\Gamma_p} \\
&\qquad \leq C(\omega) \left[h \left(\|E\|_1 + \|curl\ E\|_1 + \|H_2\|_1\right)\right. \\
&\qquad \left. + h^{1/2} \left(\|E\|_1 + \|u^s\|_{2,\Omega_p} + \|u^f\|_{1,\Omega_p} + \|\nabla \cdot u^f\|_{1,\Omega_p}\right)\right] .
\end{aligned}$$

5 NUMERICAL EXPERIMENTS FOR 2D SEISMOELECTRIC MODELING

Synthetic seismoelectrograms can aid in the understanding and interpretation of the signals generated by electrofiltration. A simple model consists of a thin clay aquitard layer (1 m) which is surrounded by sand (see Fig. 1).

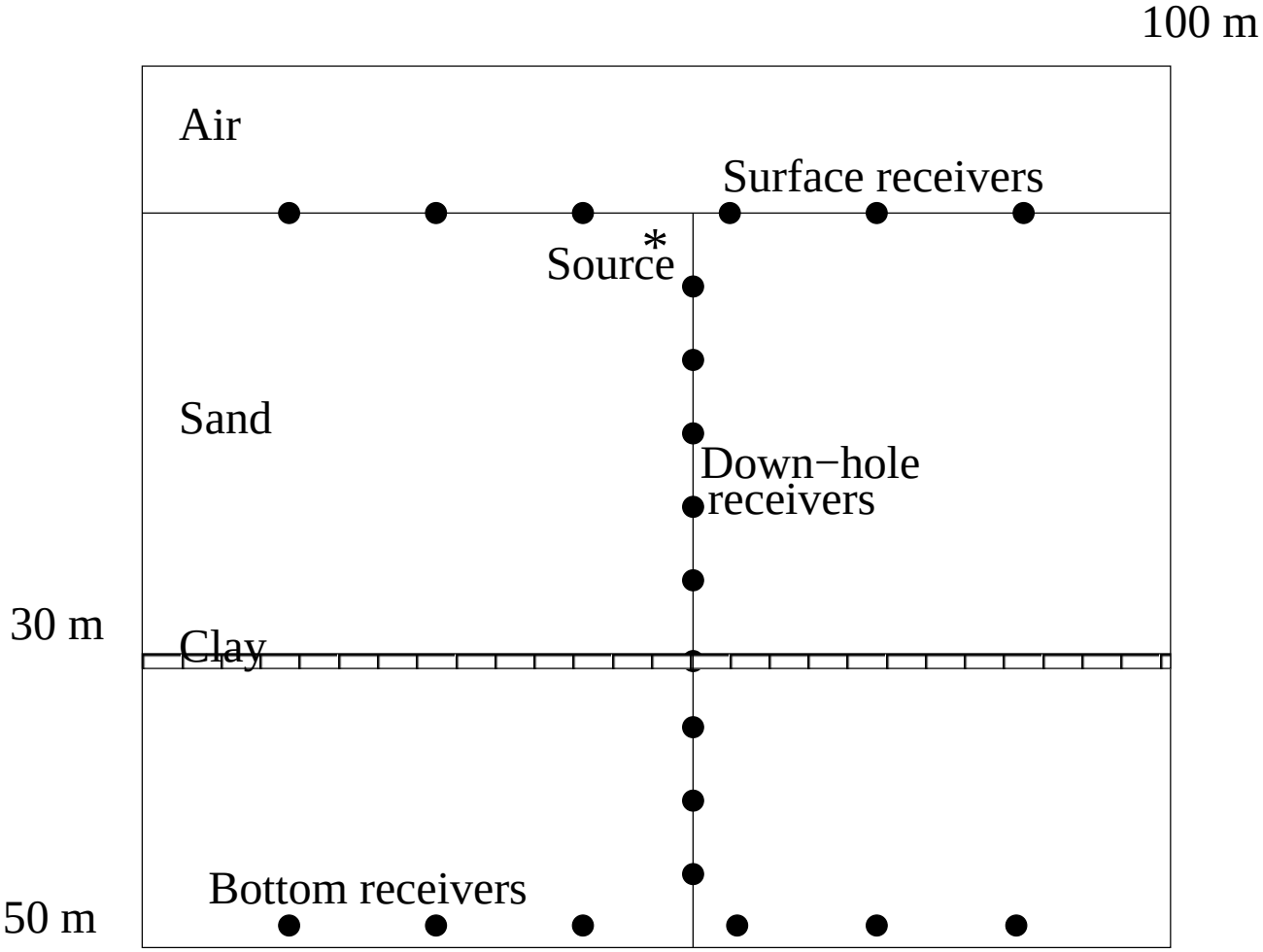

Figure 1: Geometry for a thin aquitard layer model.

The observation points are located at the surface, at 50 m depth and in a well. The distance between adjacent receivers is 5 m in the horizontal direction and 1 m downhole. The main physical parameters chosen are given in Table 1 and are taken from Haines and Pride (2006) . The pore fluid is water and their properties are: ρ_f=1000 Kg/m^3, η=10^{-3} Kg/(m s) and K_f=2.2

GPa. The density of the solid grains is ρ_s=2600 Kg/m^3. The water salinity is low, C_e=0.001 mol/l.

Material	σ [S/m]	ϕ	V_P [m/s]	V_S [m/s]	K_s [GPa]	κ_0 [m^2]	L_0	Q
Sand	0.01	0.30	1860	314	35	10^{-11}	4.95 10^-8	80
Clay	0.05	0.10	2300	406	25	10^-16	1.26 10^-9	80

Table 1: Material properties.

The calculation used a 1008x504 grid with a grid size δx_1=δx_2=0.13 m and 105 frequency samples with a frequency step size of 3.81 Hz. The time dependence of the source is given by a Ricker wavelet with a central frequency equal to 200 Hz. The simulation required about 3 hours of computation , running on 12 processors of the Steele cluster (RCAC, Purdue University).

The coseismic field is generated by the relative fluid-rock motion that accompanies the seismic P-waves. This field is indicated by "CS" in Fig. 2. Moreover, a portion of the seismic wave is converted to Biot slow wave at the interfaces that is rapidly attenuated but it creates another relative fluid-rock motion. This effect is the flat interface response labeled by "IR" that arrives at the same time, independent of offset. Electric fields for the x-component collected by receivers located on surface and in depth are shown on the left and right sides of Fig. 2, respectively.

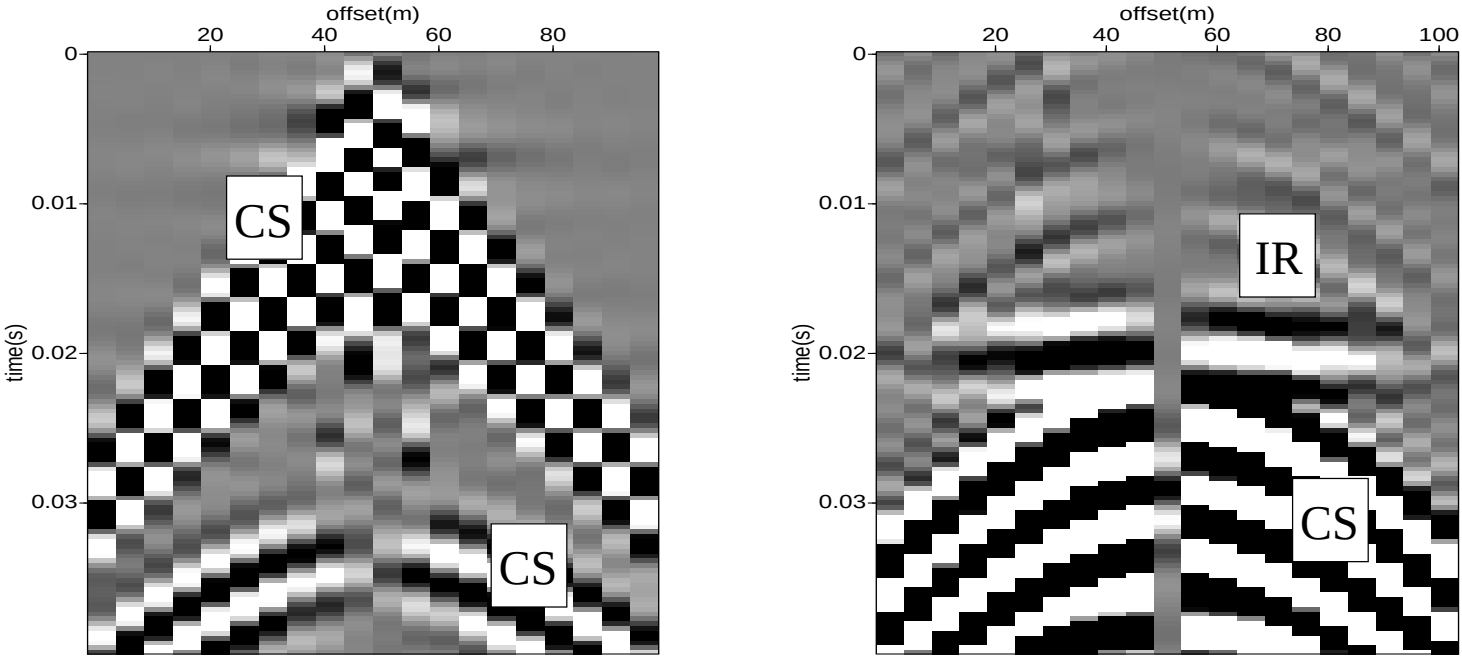

Figure 2: Synthetic seismoelectrograms.

In a surface seismoelectric measurement, the interface response arrives at the same time that the coseismic energy making it difficult to identify. However, in the bottom geometry gather the interface response is arriving before the coseismic field. Some clues to distinguish "IR" from coseismic arrivals and background noise are: (a) the signal arrives without typical seismic

moveout, (b) the signal is generated from the first Fresnel zones of seismic waves centered below the source, (c) the signal arrives in approximately one half the time required for a seismic signal and (d) the signal changes polarity on both sides of the position of the source. Different kinds of filters will be necessary to improve the signal-to-noise ratio.

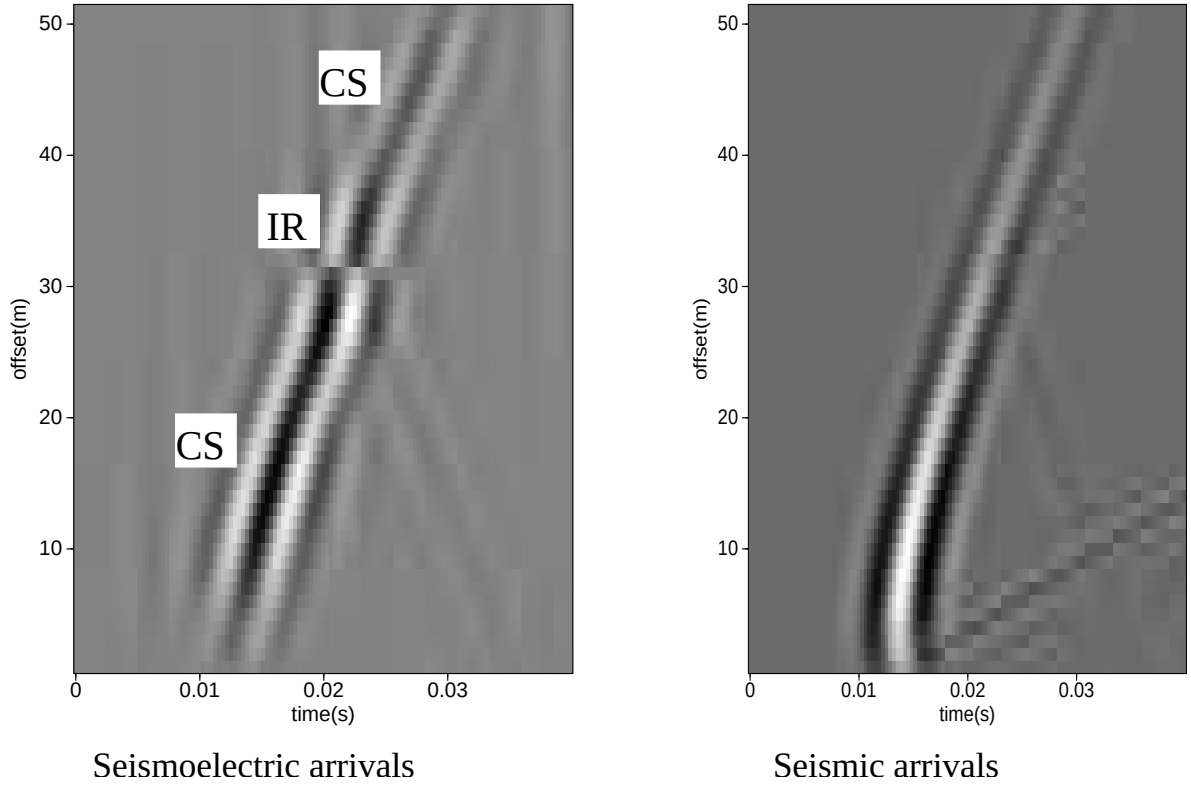

Figure 3: Comparison of seismoelectrograms and seismograms for down-hole receivers.

Fig. 3 shows a down-hole receiver array for a well located 15 m away from the source. Seismoelectric (electric field) and seismic signals (seismic waves) are plotted with horizontal time axis and vertical depth axis. Coseismic and seismic fields are associated with identical arrival times. It is also possible to see the coseismic field of the reflected P-wave. Besides, interface response generated at the thin layer propagates as an electromagnetic wave and arrives nearly simultaneously at separated receivers.

6 CONCLUSIONS

In the present paper, a finite element procedure, used to model conversion between mechanical and electromagnetic energy, is defined. The seismic source generates P and SV waves giving rise to transverse-magnetic fields (PSVTM-mode).

The equations were solved in space-frequency domain by an iterative domain decomposed finite element method for which apriori error estimates can be established. The algorith has been implemented on parallel architectures with MPI as the communication protocol.

Qualitative analysis of the results indicates that interface response can be identify, but in general, it is necessary enhance signal-to-noise ratio by filters. It is important to verify that the continuous events on the recorded data are not a processing artifact.

REFERENCES

Biot M. Theory of deformation of a porous viscoelastic anisotropic solid. *J. Appl. Physics*, page 459, 1956a.

Biot M. Theory of propagation of elastic waves in a fluid-saturated porous solid. ii. high frequency range. *J. Acoust. Soc. Amer.*, page 179, 1956b.

Biot M. Mechanics of deformation and acoustic propagation in porous media. *J. Appl. Physics*, (4):1482, 1962.

Block G. and Harris J. Conductivity dependence of seismoelectric wave phenomena in fluid-saturated sediments. *J. Geophys. Res.*, page B01304, 2006.

Douglas Jr. J., Santos J., Sheen D., and Ye X. Nonconforming galerkin methods based on quadrilateral elements for second order elliptic problems. *RAIRO Mathematical Modelling and Numerical Analysis (M2AN)*, 33:747, 1999.

Gassmann F. Uber die elastizität poröser medien. *Vierteljahrsschrift der Naturforschenden Gessellschaft in Zurich*, page 1, 1951.

Girault V. and P. R. *Finite Element Methods for Navier-Stokes Equations*. Springer–Verlag, Berlin, 1986.

Haartsen M. and Pride S. Electroseismic waves from point sources in layered media. *J. Geophys. Res.*, page 24745, 1997.

Haines S. and Pride S. Seismoelectric numerical modeling on a grid. *Geophysics*, 71(6):57, 2006.

Han Q. and Wang Z. Time-domain simulation of sh-wave-induced electromagnetic field in heterogeneous porous media: A fast finite element algorithm. *Geophysics*, (2):448, 2001.

Hornbostel S. and Thompson A. Waveform design for electroseismic exploration. *Geophysics*, 72(2):Q1–Q10, 2007.

Liu H., Anderson D., and Kanamori H. Velocity dispersion due to anelasticity; implications for seismology and mantle composition. *Geophys. J. R. Astr. Soc.*, page 41, 1976.

Mikhailov O., Haartsen M., and Toksoz M. Electroseismic investigation of the sallow subsurface: Field measurements and numerical modeling. *Geophysics*, page 97, 1997.

Mikhailov O., Queen J., and Toksoz M. Using borehole electroseismic measurements to detect and characterize fractured (permeable) zones. *Geophysics*, page 1098, 2000.

Monk P. and Parrot A. A dispersion analysis of finite element methods for maxwell's equations. *SIAM J. Sci. Stat. Comput.*, (4):916, 1994.

Nedelec J. Mixed finite elements in r^3. *Numer. Math.*, 35:315, 1980.

Pain C., Saunders J., Wortington M.H., Singer J., Stuart-Bruges W., Mason G., and Goddard A. A mixed finite element method for solving the poroelastic biot equations with electrokinetic coupling. *Geophys. J. Int.*, page 592, 2005.

Pride S. Governing equations for the coupled electromagnetics and acoustics of porous media. *Physical Review B*, 50:15678, 1994.

Pride S. and Haartsen M. Electroseismic wave properties. *J. Acoust. Soc. Amer.*, page 1031, 1996.

Ravazzoli C. and Santos J. A theory for wave propagation in porous rocks saturated by two-phase fluids under variable pressure conditions. *Bollettino di Geofisica teorica ed applicata*, (4):261, 2005.

Raviart P. and Thomas J. *A mixed finite element method for second order elliptic problems. Lecture notes in Mathematics.*, volume 606. Springer-Verlag, Berlin, New York, 977.

Santos J. Finite element approximation of coupled seismic and electromagnetic waves in fluid-

saturated poroviscoelastic media. *Numerical Methods for Partial Differential Equations*, 2010.

Santos J., Douglas Jr J., Morley M., and Lovera O. Reflection and transmission coefficients in fluid-saturated porous media. *J. Acoust. Soc. Amer*, page 1911, 1992.

Santos J., Douglas Jr. J., Morley M., and Lovera O. Finite element methods for a model for full waveform acoustic logging. *IMA journal of Numerical Analysis*, page 415, 1998.

Santos J. and Sheen D. Finite element methods for the simulation of waves in composite saturated poroviscoelastic materials. *SIAM J. Numer. Anal*, (1):389, 2007.

Sheen D. A generalized green's theorem. *Appl. Math.Lett.*, page 95, 1992.

Sheen D. Approximation of electromagnetic fileds: Part i. continuous problems. *SIAM J. Appl. Math.*, page 1716, 1997.

Thompson A. Electromagnetic-to-seismic conversion: Successful developments suggest viable applications in exploration and production. In *75th SEG Annual Meeting Expanded Abstracts*. SEG, Houston, 2005.

Thompson A. and Gist G. Geophysical applications of electrokinetic conversion. *The leading edge*, 12:1169, 1993.

White B. Asymptotic theory of electroseismic prospecting. *SIAM J. Appl. Math.*, (4):1443, 2005.

White B. and Zhou M. Electroseismic prospecting in layered media. *SIAM J. Appl. Math*, (1):69, 2006.